Hindawi Publishing Corporation
Shock and Vibration
Volume 2015, Article ID 846308, 14 pages
http://dx.doi.org/10.1155/2015/846308

Research Article

Acoustic Emission Signal Recognition of Different Rocks Using Wavelet Transform and Artificial Neural Network

Xiangxin Liu,[1,2] Zhengzhao Liang,[2] Yanbo Zhang,[1] Xianzhen Wu,[3] and Zhiyi Liao[2]

[1] *College of Mining Engineering, Hebei United University, Tangshan, Hebei 063009, China*
[2] *School of Civil Engineering, Dalian University of Technology, Dalian 116024, China*
[3] *School of Resources and Engineering, Jiangxi University of Science and Technology, Ganzhou 341000, China*

Correspondence should be addressed to Zhengzhao Liang; liangzz@dlut.edu.cn

Received 7 August 2014; Revised 26 October 2014; Accepted 28 October 2014

Academic Editor: Ting-Hua Yi

Different types of rocks generate acoustic emission (AE) signals with various frequencies and amplitudes. How to determine rock types by their AE characteristics in field monitoring is also useful to understand their mechanical behaviors. Different types of rock specimens (granulite, granite, limestone, and siltstone) were subjected to uniaxial compression until failure, and their AE signals were recorded during their fracturing process. The wavelet transform was used to decompose the AE signals, and the artificial neural network (ANN) was established to recognize the rock types and noise (artificial knock noise and electrical noise). The results show that different rocks had different rupture features and AE characteristics. The wavelet transform provided a powerful method to acquire the basic characteristics of the rock AE and the environmental noises, such as the energy spectrum and the peak frequency, and the ANN was proved to be a good method to recognize AE signals from different types of rocks and the environmental noises.

1. Introduction

Many kinds of rocks are fracturing due to human activity or geological process. It is well known that elastic waves are emitted from rock mass during their fracturing process. Therefore, various symptoms related to the breakdown of rock mass can be detected by the acoustic emission (AE) technique [1, 2].

Rock mass is an environmental geological body; it is formed in a certain environment by mineral composition and structural plane due to movement of geological structures and complex atmospheric environment. Different types of rocks contain different kinds of minerals and different geological structures, such as joints and microcracks. The fracture involves debonding and slipping between the grains, minerals, and geological structures in rocks. Each AE signal is an indication that some part of the released energy due to the rock crack propagation is transformed into an elastic wave. Therefore, different types of rocks will generate different types of elastic waves. Laboratory experiments and field monitoring are often conducted to investigate the characteristics of rock AE signals. These AE signals are often mingled with electric signals and artificial noises. Therefore, how to distinguish these signals becomes a significant topic in AE investigations [3–5].

Monitoring techniques and artificial intelligence algorithm have been widely used in rock slopes and tunnels [6, 7], concrete dams [8, 9], and high-rise structures [10, 11]. Artificial neural network (ANN) has some capability of learning from examples through iteration, without requiring prior knowledge of the relationships between the process parameters. The major benefits in using ANN are the excellent management of uncertainties, noisy data, and nonlinear relationships. Neural network modeling has become increasingly accepted and is an interesting method for application to the AE technique [4, 5, 12–15].

Many authors have conducted AE investigations using ANN. Kwak and Song constructed a neural network to achieve an intelligent diagnosis for chattering vibration and burning phenomena on grinding operation. The item of static power, dynamic power, peak of RMS, and peak of FFT has been used as an input feature of the neural network to diagnose the grinding faults [12]. Samanta and Al-Balushi presented a procedure for fault diagnosis of rolling element

(a) RMT-150C (b) SAEU2S

Figure 1: The servo controlled rock mechanical test machine RMT-150C and AE monitoring system SAEU2S.

bearings through ANN. The time-domain vibration signal of the rotating machinery with normal and defective bearings has been used as the input feature of the ANN. The results showed that the effectiveness of the ANN can diagnose the physical condition of machine [16]. Samanta et al. compared the performance of bearing fault detection by ANNs and support vector machines (SMVs) [17]. Kim et al. trained an ANN to recognize the stress intensity factor in the time interval of microcrack to fracture by AE measurement [18]. Hill et al. used the AE flaw growth activity to train a back-propagation neural network to predict the ultimate strengths in the remaining six specimens [19]. However, few investigations can be found by using ANN to distinguish rock AE signals and determine their characteristics for different rock types.

The objective of the current research was to develop a neural network for the prediction of rock types or other noises from their AE measurements. The AE signals were recorded in the rock failure process under uniaxial loading. The wavelet analysis helped to obtain the basic parameters of the AE signals of the rocks and the environmental noises. These parameters were used to establish input layers in the ANN. The trained ANN was applied to predict rock types and noise types. The predictions obtained from the ANN are in good agreement with the laboratory experiments. The ANN based on AE measurement can be used to distinguish different rock AE signals and predict different rock specimens in rock engineering.

2. Experiment Preparation and Methods

2.1. Laboratory Experiments. A total of four types of rocks were selected to conduct uniaxial compression. To guarantee the diversity of the rock types, these rock specimens were collected from four mines in China. The granulite specimens were obtained from a gold mine in Fujian province, the limestone specimens were from a tin ore mine in Guangxi province, the granite specimens were from an open pit central in Jiangxi province, and the siltstone specimens were obtained from a mine in the south of Jiangxi province.

All the mechanical tests were conducted on a servo controlled rock mechanical machine RMT-150C (Figure 1(a)). This machine has a visualization operation platform based on Windows, and it can record the load, stress, and strain during the rock failure process.

An AE monitoring system SAEU2S with 8 parallel detection channels was applied to collect AE events in the compression (Figure 1(b)). Each channel with an AE sensor, a preamplifier, and an acquisition card can collect the parameters of AE events, such as the amplitude, energy, and counts.

2.2. AE Signals. AE signals as well as electronic noises were recorded and processed during the rock fracturing. The AE signals in time domain and frequency domain were analyzed in this section.

2.2.1. The AE Signals in Time Domain. Different rocks generated different AE signals in time domain under the same stress condition. AE counts, cumulative AE counts, energy, rise times amplitudes, event rates, and energy rates are often used to describe the AE features in time domain. Cumulative AE counts can reflect internal damage in the rock specimens.

According to curves of cumulative AE counts, axial stress, and time (Figure 2), the curves can be divided into four periods: pre-linear period, linear period, post-peak and nonlinear period, and residual strength period.

All the AE signals of the specimens show a sudden jump before their final failure, accompanied by a stress drop. The granulite specimens show a sudden increase before failure without precursors. The stress for the granite specimens lasted many times of stress buildup and stress release before final failure. The AE counts for the limestone specimens increased gradually before the peak strength points. The siltstone specimens demonstrated an obvious residual failure process, and the cumulative AE counts reached the peak point after the peak strength points.

The granulite, limestone, and granite specimens showed a hard and brittle failure mode and their curves for the post-peak period were not obtained. The soft siltstone showed slight plastic failure mode.

2.2.2. The AE Signals in Time Domain in Frequency Domain. A continuous wavelet transform (CWT) is used to divide a continuous-time function into wavelets. Unlike Fourier transform, the continuous wavelet transform possesses the

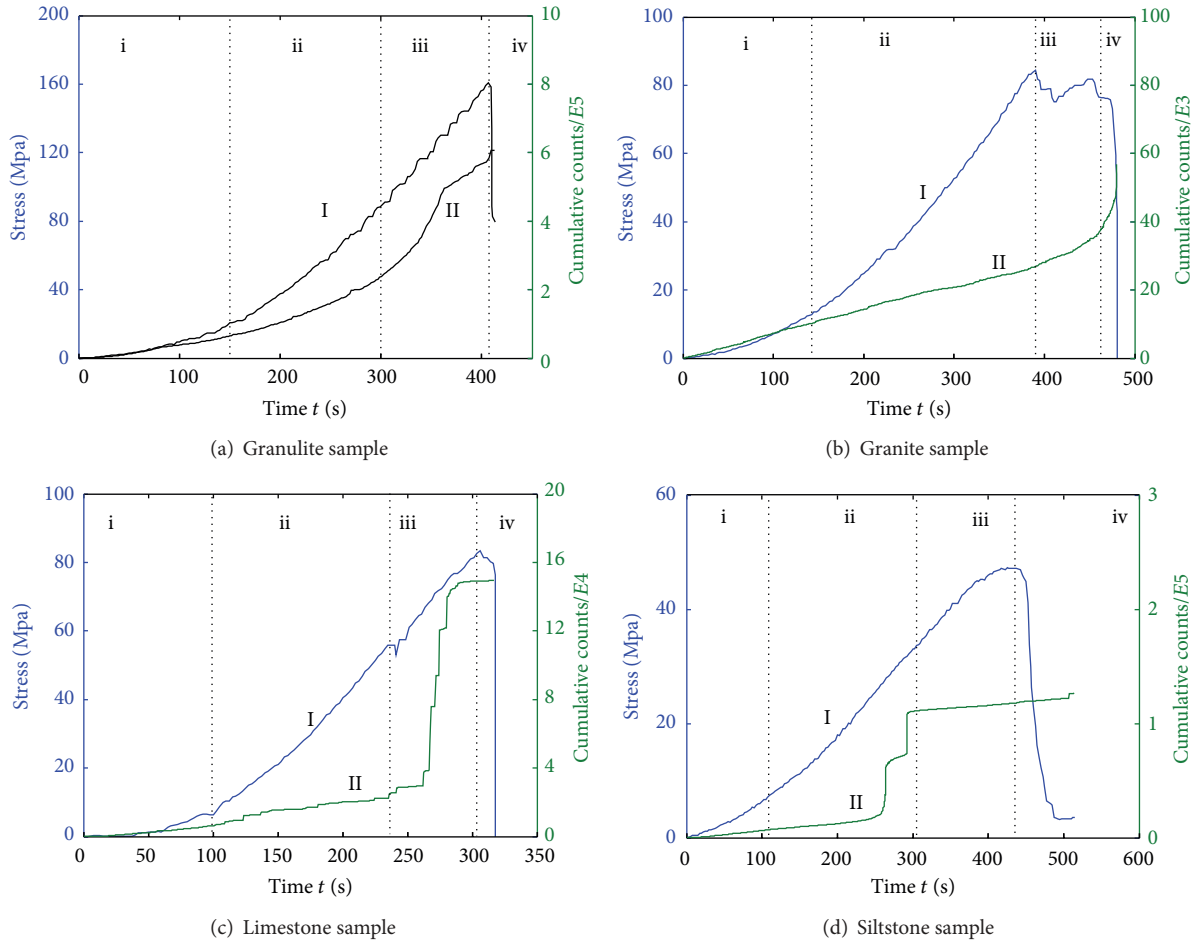

(a) Granulite sample

(b) Granite sample

(c) Limestone sample

(d) Siltstone sample

Figure 2: Curves of cumulative counts, axial stress, and load time (I: stress-time curve; II: cumulative counts-time curve).

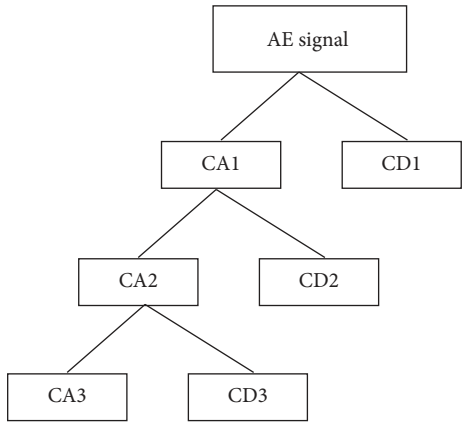

Figure 3: Topology structure of wavelet decomposition with 6 layers.

ability to construct a time-frequency representation of a signal that offers very good time and frequency localization. CWT is very efficient in determining the damping ratio of oscillating signals. CWT is also very resistant to the noise in the signal.

According to Mallat theory, the fast wavelet transform algorithm, the signal function can be decomposed into the low frequency component and the high frequency component under the scale j of the wavelet packets transform:

$$\begin{aligned} f(n) &= A_0 f(n), \\ A_0 f(n) &= A_1 f(n) + D_1 f(n), \\ &\vdots \\ A_{J-1} &= A_J f(n) + D_J f(n), \end{aligned} \tag{1}$$

where $f(n)$ is the signal function, A_i is the low frequency component coefficient, and D_i is the high frequency component coefficient. So the signal function can be described as follows under the scale J:

$$f(n) = A_J f(n) + \sum_{j=1}^{J} D_j f(n). \tag{2}$$

A topology structure of a wavelet transform with 3 layers is shown in Figure 2. Figure 3 shows topology structure of wavelet decomposition with 6 layers.

Table 1: Energy ratio of the wavelet transformed AE signals in failure.

Decomposition layers	CA6	CD6	CD5	CD4	CD3	CD2	CD1	Band/kHz
Frequency layers/kHz	0~78	78~156	156~312.5	312.5~625	625~1250	1250~2500	2500~5000	
Energy ratio/%								
Granulite	0.61645	4.7345	15.846	74.723	4.0579	0.022976	0.0018851	[156, 625]
Granite	89.339	9.9742	0.47787	0.14506	0.016137	0.16799	0.031258	[0, 78]
Limestone	59.835	35.511	2.4313	1.926	0.26136	0.013166	0.022664	[0, 156]
Siltstone	52.215	44.053	3.5185	0.17952	0.011493	0.0076762	0.015349	[0, 156]

Nowadays wavelet analysis is widely used to analyze nonstationary random signals [20]. The wavelet analysis is a time-frequency localized analysis method, in which the window size is fixed but its shape can be changed, and time- and frequency-window can also be changed, which means the low frequency part with higher frequency resolution and lower time resolution and the high frequency part with a higher time resolution and lower frequency resolution [20]. The wavelet analysis can decompose AE signals both in frequency domain and in time domain. The wavelet analysis provides a kind of adaptive time and frequency domain localization analysis method.

Figure 4 shows relationship between frequency and amplitude of the AE signals in rock final failure stages. The dynamical damage processes and characteristics of different rocks (granite, granulite, siltstone, and limestone) under the stress condition were obtained. It is found that the transformed AE signals for different rock types were different.

The frequency distribution reflected rock fracture and associated AE characteristics. As shown in Figure 4 and Table 1, the frequency domain of the granulite specimens was mainly distributed in CD5 and CD4, taking up more than 90% of all the frequency bands. Most of the frequency of the granulite signals was located in high frequency bands [156, 625 kHz]. The frequency domain of the granite specimens was distributed in low bands from CD1 to CD6, and CA6 took up above 89% of all the signals, which ranged in [0, 78 kHz]. Most of the granite AE signals belonged to low frequency bands, while the AE signals of the limestone specimens mainly concentrated in the frequency of CA6 (59.835%) and CD6 (35.511%).

2.3. The Artificial Neural Network. The artificial neural network can be seen as a set of parallel processing elements, and the suitable mathematical methods can be used to change the weights and thresholds to perform specific functions. The BP neural network can figure out each layer's error derivatives by using the back-propagation algorithm according to the generated weight matrices and threshold matrices. And then, BP adjusts corresponding matrices on the basis of error derivatives and square error sum to approach the mapping relation between the system input variables and output variables step by step. The typical structure of a BP neural network is shown in Figure 5. It has one input layer, one or more hidden layers, and one output layer, with each layer consisting of one or more neurons.

The number of neurons (m) in the input layer is the same as the number of mechanical parameters to be solved, and the number of neurons (n) in the output layer is the number of the measured displacements. Usually, only one hidden layer is needed. The number of neurons (p) in the hidden layer can be specified either manually or by an optimization method. The training specimens are often used to adjust the weight values by making the summed squared error between the displacements from numerical simulation and those from BP network a minimum. For the training specimens, the input parameters can be prepared by the parameter experiment design method, while the corresponding output parameters can be prepared by numerical simulation.

The calculating procedure of a three-layer BP neural network is shown in Figure 6. W_1 and b_1 are weight matrix and threshold matrix between the input layer and the hidden layer, respectively; W_2 and b_2 are weight matrix and threshold matrix between the hidden layer and the output layer, respectively; function f is the transfer function between two adjacent layers. Three transfer functions, including Tan-Sigmoid transfer function (*tansig*), Log-Sigmoid transfer function (*logsig*), and linear transfer function (*purelin*), are the most commonly used transfer functions for multilayer networks.

3. Results and Discussion

3.1. Mechanical Experiment Results. Figure 7 shows typical fracture patterns for these four types of rock specimens. These rock specimens demonstrated different fracture patterns under uniaxial compression. A shear crack was formed in the granulite specimen, and the rupture is a typical single shear failure mode. Some thin flakes spalled from the granite specimen vertically, and the failure mode is a typical splitter failure. Several parallel cracks occurred in the limestone specimen, which run through the whole specimen from the bottom to the top, accompanied by some small cracks. It had the same tensile failure mode as granite specimen. The siltstone presented a typical slightly plastic rock. The cracks in the siltstone specimen developed relatively slow, and an X fracture pattern was observed on the surface, indicating a typical shear failure mode.

The four types of rock specimens have different failure modes. On the one hand, different types of rocks have different distribution of mineral particle size and hardness of mineral grains and different microgeological structure. On

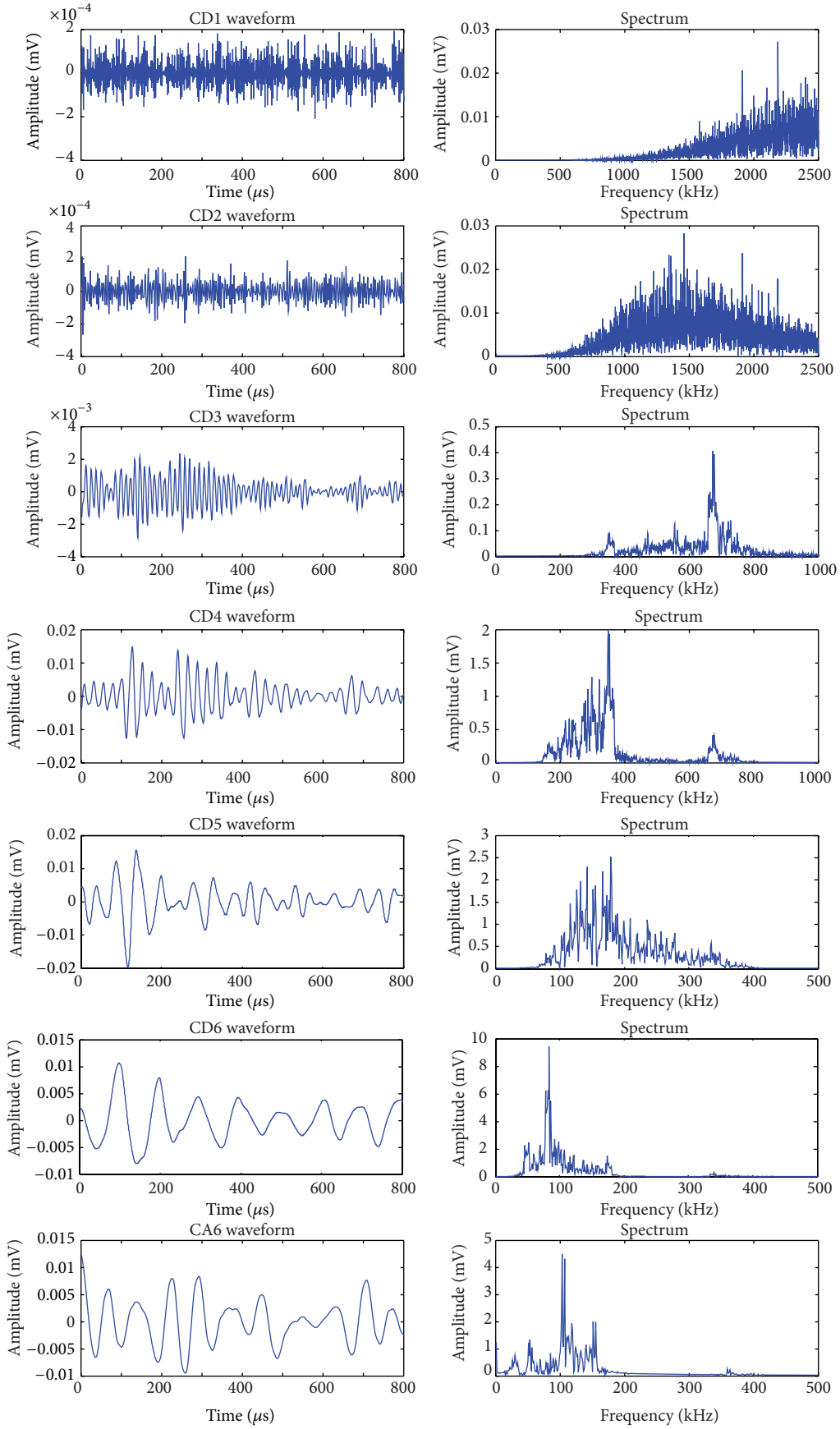

(a) Granulite

Figure 4: Continued.

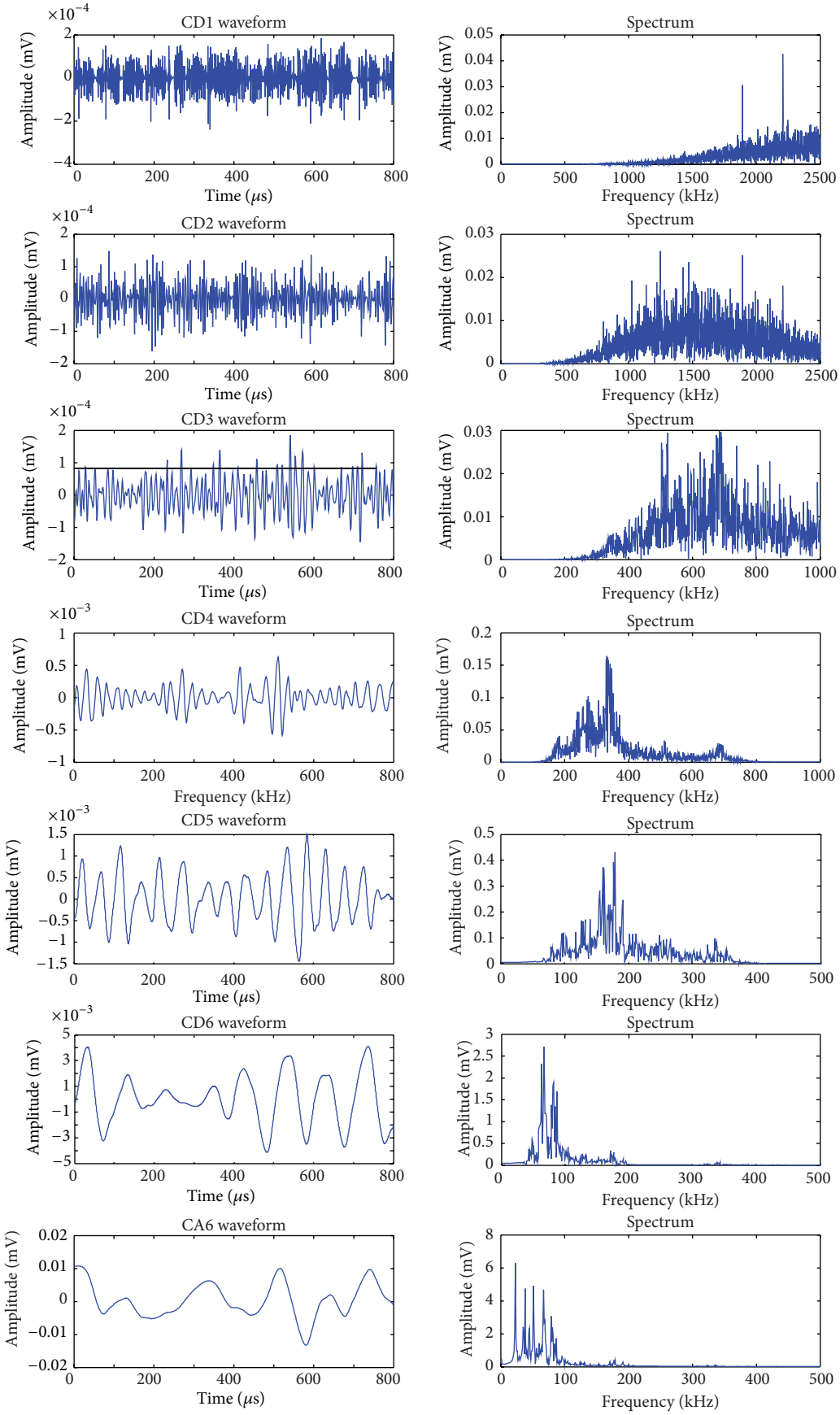

(b) Granite

Figure 4: Continued.

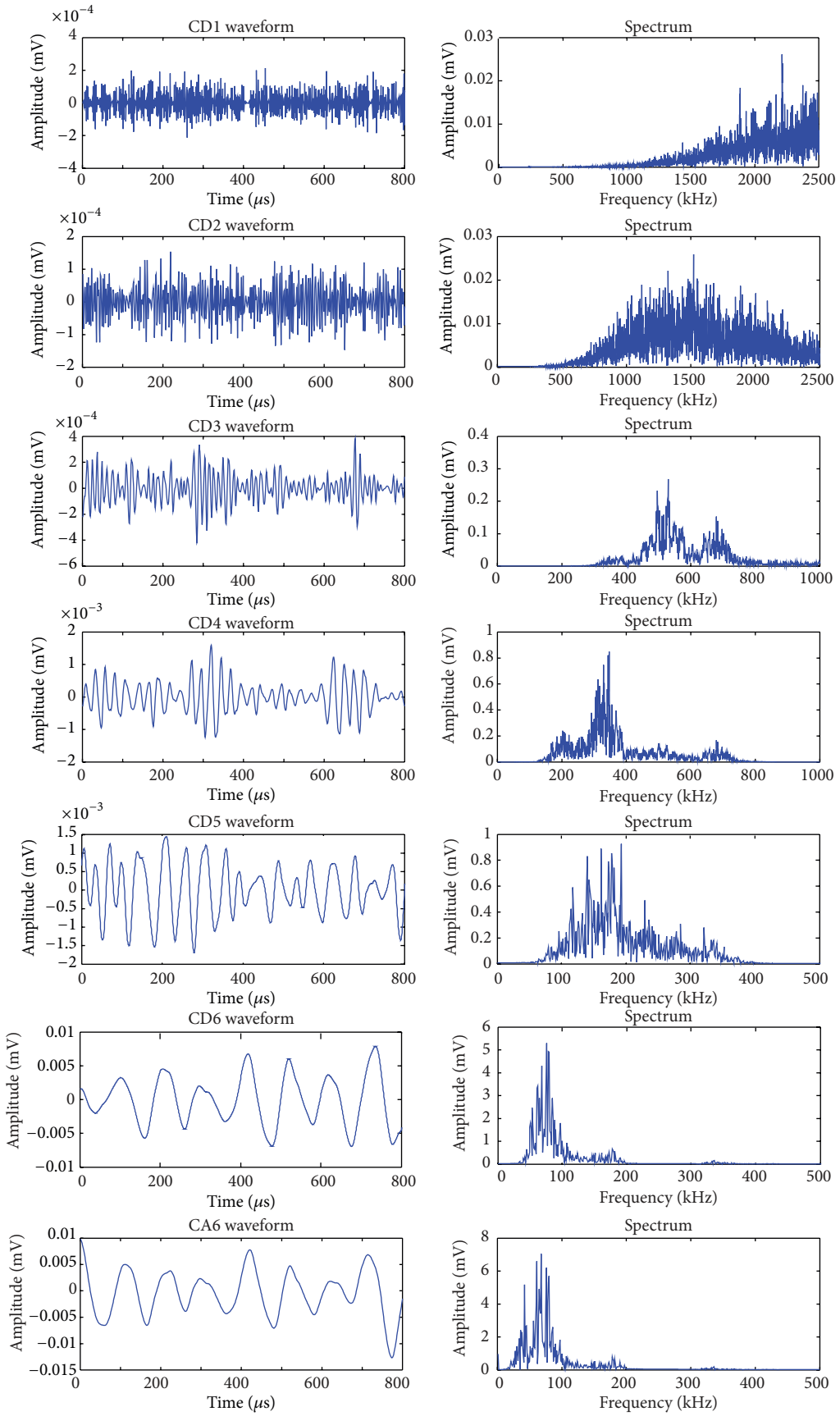

(c) Limestone

Figure 4: Continued.

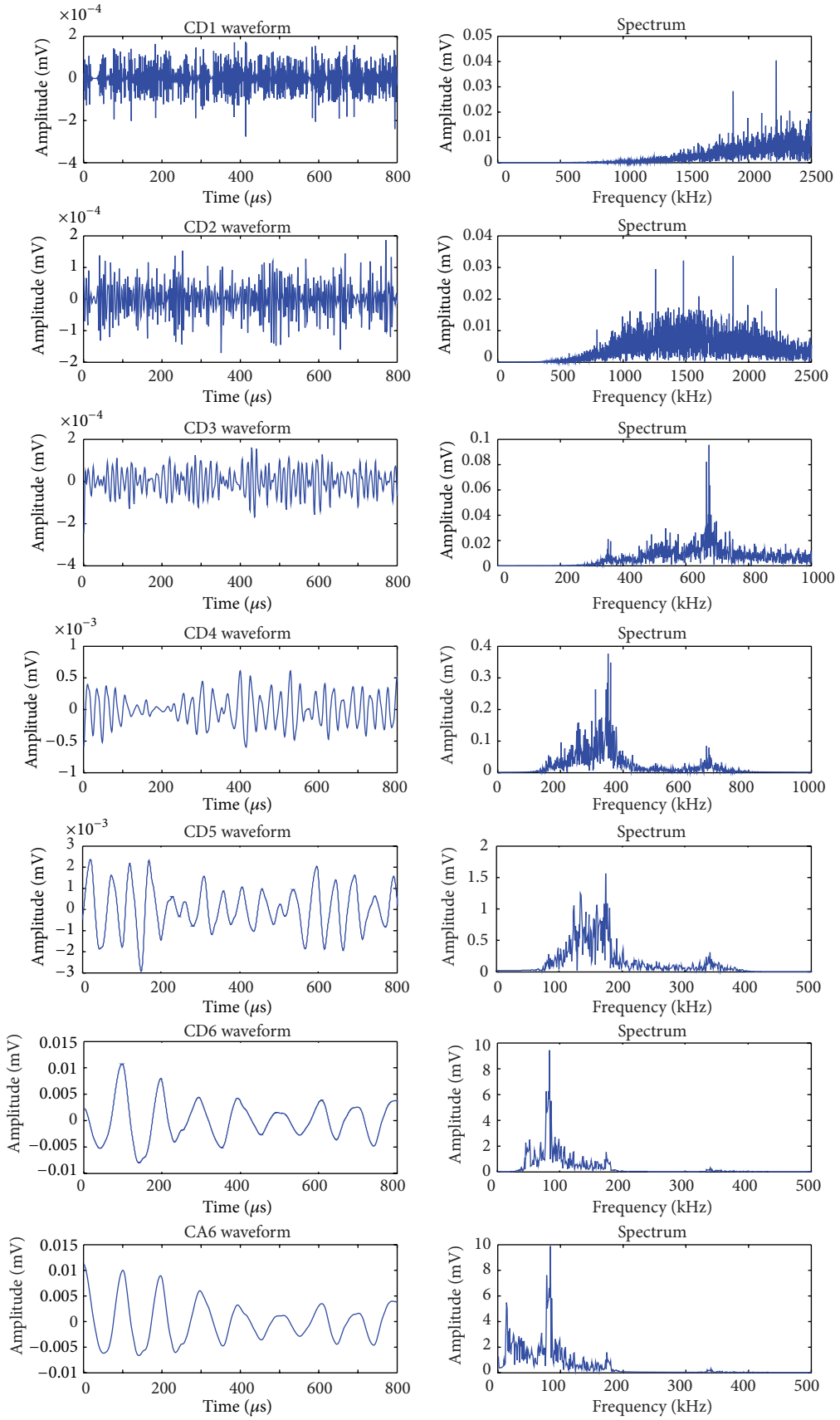

(d) Siltstone

Figure 4: Six layers of the wavelet decomposition for the rock specimens.

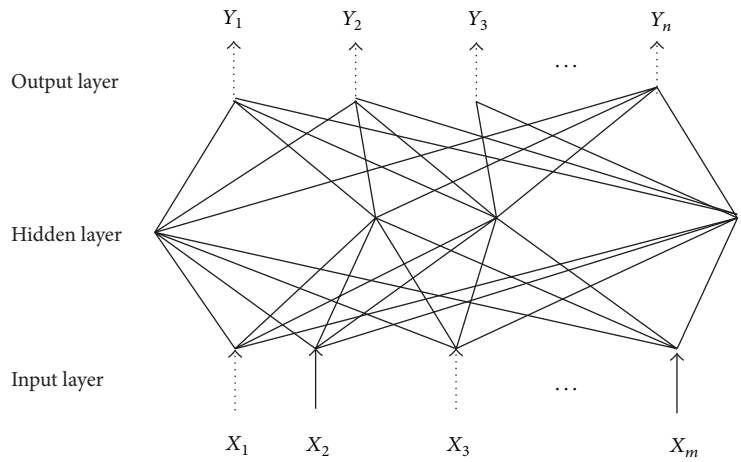

Figure 5: Typical structure of a BP neural network [18].

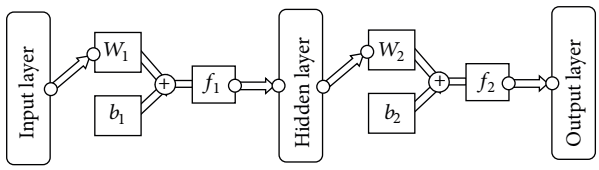

Figure 6: Flow chart of BP neural network.

the other hand, different rock contains different properties and scales of weakness structural plane.

3.2. AE Characteristics. Figure 8 shows the curves of the accumulated AE counts as the load increased for the four typical specimens. Figure 9 shows the curves of the AE rate and the load for the specimens. It can be observed that the limestone specimen and the granite specimen produced more AE events than the siltstone specimen and the granulite specimen in beginning loading stage. However, the AE rates of the granite and granulite specimens were higher than the limestone and siltstone specimens. The granite specimen generated the smallest number of the AE events, whereas it had the largest number of the AE rates. The siltstone did not generate a large number of the AE events before the sudden burst failure.

Figure 10 shows the wavelet transformed energy spectrum coefficient of the rock specimens. It can be observed that the spectrum coefficient of the granulite, granite, and limestone specimens was mainly distributed in CA6, CD6, CD5, and CD4 bands. The distribution for the siltstone specimen was distributed in CA6 and CD6 bands.

Table 2 lists the distribution of the frequency band in each layer. The frequency range of the AE signals could be determined by the wavelet transform. The frequency of the hard and brittle rock (the granulite, granite, and limestone specimens) ranged from 0 kHz to 625 kHz. The siltstone belongs to a moderate strength and slightly plastic rock, and the frequency ranged from 0 kHz to 312.5 kHz in a narrower band.

4. The Recognition of the AE Signals Using the ANN

4.1. ANN Structure. The numbers of the neurons in the input layer, output layer, and the hidden layer and a proper transfer function should be determined in a typical ANN structure.

Input layer vector: there were 11 input neurons in the ANN model as shown in Table 3: rise time ($X1$), ring count ($X2$), energy ($X3$), duration time ($X4$), amplitude ($X5$), peak frequency ($X6$), the CA6 value of the wavelet decomposition ($X7$), the CD6 value of the wavelet decomposition ($X8$), the CD5 value of the wavelet decomposition ($X9$), the CD4 value of the wavelet decomposition ($X10$), and the CD3 value of the wavelet decomposition ($X11$).

Output layer vector: there were three neurons in the output layer. The output parameters ($y1$, $y2$, and $y3$) should be either one or zero. Their combined value indicated the signal types (Table 4). For example, the output value 001 ($y1 = 0$, $y2 = 0$, and $y3 = 1$) predicted the signal generated by a granulite specimen.

According to the number of the input neurons and the output neurons, the number of the neurons in the hidden layer can be obtained as follows [19]:

$$n_1 = \sqrt{n + m} + a, \tag{3}$$

where n_1, m, and n are the numbers of the neurons in the hidden layer, the input layer, and the output layers, respectively, and a is a constant between 0 and 10. Since the input vector dimension was set to be 11 and the output vector dimension was set to be 3, n_1 could range from 4 to 14. The number of the neurons in the hidden layer was set to be 14 in the ANN model.

Three transfer functions, including Tan-Sigmoid transfer function (*tansig*), Log-Sigmoid transfer function (*logsig*), and linear transfer function (*purelin*), are the most commonly used transfer functions for multilayer networks.

Two transfer functions were required in the ANN structure. The input parameters, such as the rise time, ring count, energy, duration time, and the amplitude, had been

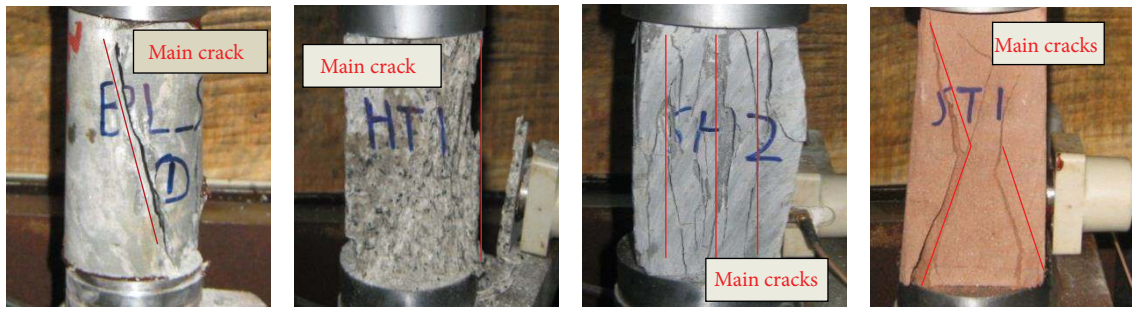

(a) Specimen BL1 (granulite) (b) Specimen HT1 (granite) (c) Specimen SH2 (limestone) (d) Specimen ST1 (siltstone)

Figure 7: Fracture patterns for the four types of rock specimens.

Table 2: The distribution of the frequency band in each layer.

	The layer of wavelet decomposition						
	CA6	CD6	CD5	CD4	CD3	CD2	CD1
Frequency range (kHz)	0~78	78~156	156~312.5	312.5~625	625~1250	1250~2500	2500~5000

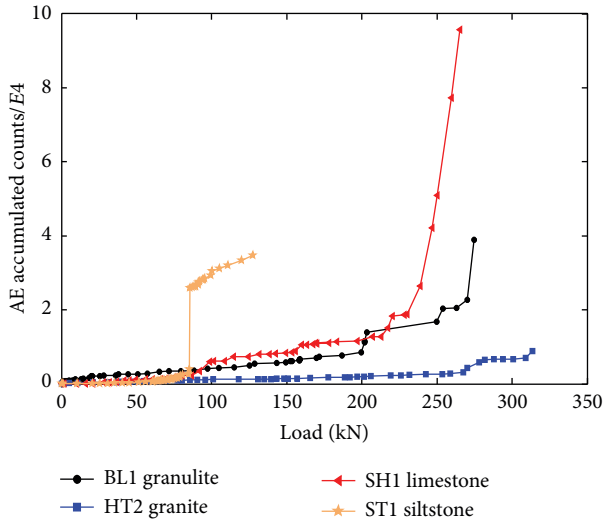

Figure 8: The curves of the accumulated AE counts and load for the four specimens.

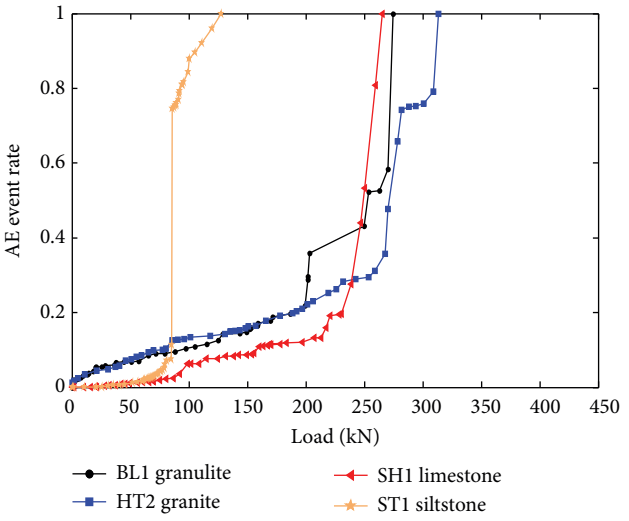

Figure 9: The curves of the AE rate and load for the four specimens.

normalized into the range $[-1, 1]$ before input into the transfer function *tansig* as arguments. Compared with the transfer function *purelin*, *logsig* was better to link the hidden layer and the output layer. After one-minute training at the 360th iterative step, the mean squared error was less than 0.005 (Figure 11). For the *purelin* function, the mean squared error did not reach 0.009 until 100,000 steps (Figure 12).

4.2. BP Network Training. Six types of elastic wave signals were considered in the ANN model, including the four types of the rocks, the electrical noise, and artificial knock noise. Totally 120 sets of the rock AE signals (30 sets of the granulite AE signals, 30 sets of the granite AE signals, 30 sets of the limestone signals, and 30 sets of the siltstone AE signals) were used for training. There were 30 sets of the electrical noise signals and 15 sets of the artificial noise signals for training. The RPROP algorithm was applied in the training, the mean squared error of the objective function was set to be 005, the maximum number of iterative steps was 100,000, and the number of independent training times was set to be more than 50. As shown in Figure 13, the mean squared error reached the specified minimum value after 374 training steps.

4.3. ANN Recognition. Some basic parameters, such as the rise time, the ring count, the energy, the duration time, and the amplitude, describing the characteristics of the AE signals, were combined as an input vector in the network. Moreover, the wavelet transform method was applied to decompose the signal waves to obtain the frequency spectrum. The decomposed energy spectra at different layers were also treated as the input parameters. The trained neural

Table 3: Input parameters and their signal types.

Rise time/$a1$	Ring count/$a2$	Energy/$a3$	Duration time/$a4$	Amplitude/$a5$	Peak frequency/$a6$	CA6 layer of wavelet decomposition/$a7$	CD6 layer of wavelet decomposition/$a8$	CD5 layer of wavelet decomposition/$a9$	CD4 layer of wavelet decomposition/$a10$	CD3 layer of wavelet decomposition/$a11$
−0.9944	−0.9946	−0.9996	−0.9955	−0.2645	0.1404	0.4449	−0.2088	−0.4542	−0.6116	0.0746
−0.9917	−0.8019	−0.9658	−0.8734	0.4908	−0.7638	−0.5627	−0.3218	0.7551	−1.0000	0.0746
−0.9981	−0.9986	−0.9998	−0.9986	−0.3013	−0.7796	−0.6560	−0.7819	−0.8793	0.6216	0.0746
−0.9907	−0.9813	−0.9981	−0.9847	−0.0919	−0.0960	0.2005	−0.1534	−0.0943	−0.8261	0.2388
−0.9986	−0.9989	−0.9997	−0.9826	−0.3833	−0.1998	−0.0113	−0.2583	−0.5884	−0.2963	0.2388
−0.9954	−0.9774	−0.9968	−0.9811	0.0835	−0.8997	−0.9157	−0.8796	−0.8954	0.8161	0.0000
−0.9995	−0.9739	−0.9961	−0.9304	0.0580	−0.7373	−0.6852	−0.7980	−0.8384	0.6148	0.0746
−0.9801	−0.9766	−0.9971	−0.9245	−0.1372	−0.4244	−0.2463	−0.5013	−0.3729	−0.1488	0.0746
−0.9958	−0.9671	−0.9957	−0.9710	0.0580	−0.2490	−0.0722	−0.2650	−0.5771	−0.2764	−0.0896
−0.9991	−0.9644	−0.9954	−0.8638	−0.1796	−0.4675	−0.3698	−0.5240	−0.7964	0.2235	0.6866
						... ...				
−0.7740	−0.7066	−0.5099	0.2520	0.9661	−1.0000	−0.9925	−0.9809	−0.2206	0.4489	−0.6567
−0.9092	−0.8845	−0.8938	−0.4225	0.8218	−0.9947	−0.9993	−1.0000	−0.9561	1.0000	−0.8358
−0.8796	−0.8671	−0.7102	−0.1123	0.9123	−0.9911	−0.9945	−0.9418	−0.4143	0.5553	−0.8358
−0.9801	−0.9842	−0.9674	−0.9293	0.7624	−0.9947	−0.9882	−0.8576	0.6103	−0.2624	−0.7015
−0.7032	−0.6484	−0.4425	0.2268	0.9349	−0.9987	−1.0000	−0.9919	−0.9503	0.9891	−0.8507

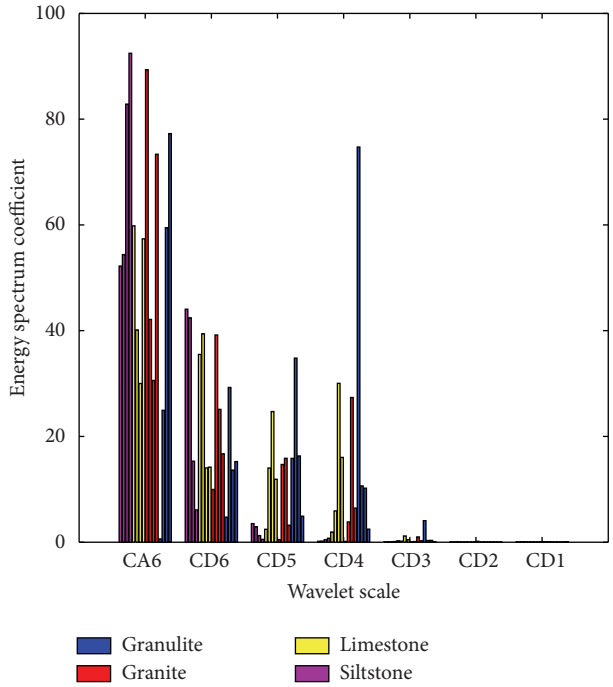

Figure 10: The distribution of the energy spectrum after the wavelet transform.

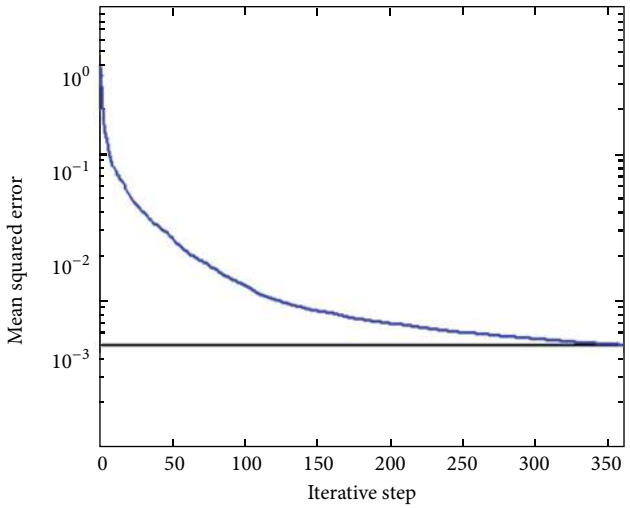

Figure 11: Convergence curve using the *logsig* function.

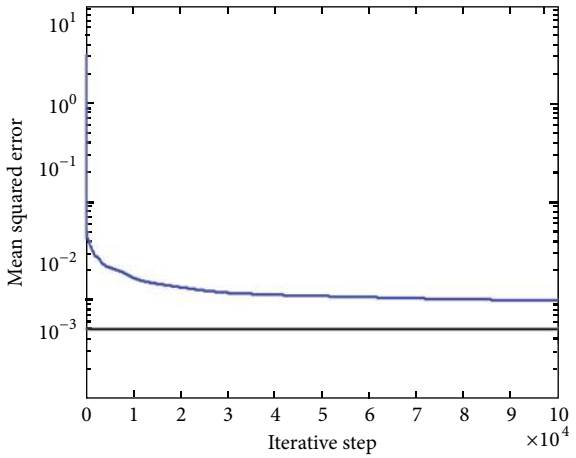

Figure 12: Convergence curve using the *purelin* function.

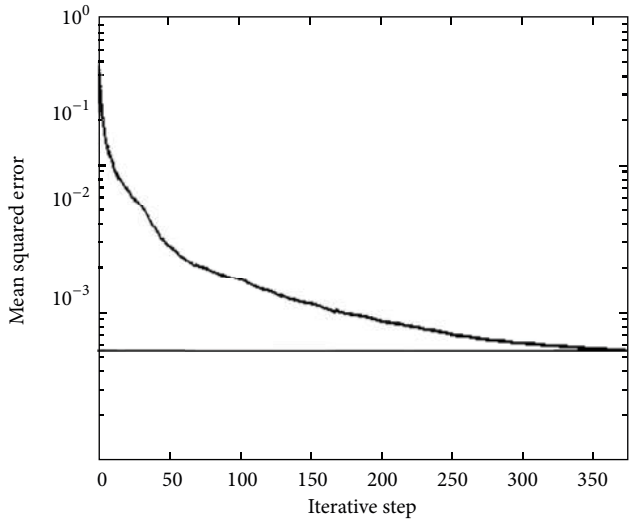

Figure 13: The convergence curve in the training.

Table 4: Output parameters and their signal types.

Signal type	$y1$	$y2$	$y3$	Output value
Granulite	0	0	1	001
Granite	0	1	0	010
Limestone	0	1	1	011
Siltstone	1	0	0	100
Electrical noise	1	0	1	101
Knock noise	1	1	0	110

network was used to predict the signal types by establishing the mapping function between the input parameters and the output parameters.

The predicted results proved that the BP neural network based on the wavelet transform analysis can achieve a high accurate ratio to recognize different rock AE signals. Table 5 listed the recognized AE signal types of the 110 sets of signals using the ANN model. There were 20 sets of the granulite signals, 20 sets of the granite signals, 20 sets of the limestone signals, and 20 sets of the siltstone signals. The average accuracy of the signal prediction for the rocks was greater than 90%. It should be noted that all the signals for the granulite, the siltstone, and electrical noises were predicted by the ANN model. Only one set of the limestone AE signals was predicted to be generated by the granulite specimens, and two sets of the granite AE signals were predicted to be generated by the siltstone specimens. Four sets of the knock noise

Table 5: Signal type prediction using the ANN.

Signal types	Signal set number	Predicted results						Accuracy
		Granulite	Granite	Limestone	Siltstone	Electrical noise	Knock noise	
Granulite	20	20	0	0	0	0	0	100%
Granite	20	0	17	0	2	0	1	85%
Limestone	20	1	0	19	0	0	0	95%
Siltstone	20	0	0	0	20	0	0	100%
Electrical noise	20	0	0	0	0	20	0	100%
Knock noise	10	0	4	0	0	0	6	60%

signals were recognized as the granite signals, indicating that the signal waves generated by the granite specimens were much similar to the artificial knock signals. Influenced by the random factors and the environmental factors, the accuracy for the artificial knock noise recognition was as low as 60%. To achieve good monitoring results, manmade noises should be reduced or eliminated in laboratory AE tests on rocks.

5. Conclusions

The wavelet transform and artificial neural network were applied to determine rock types from their AE characteristic parameters. The wavelet transform was used to decompose the AE signals, and the artificial neural network (ANN) was established to recognize the rock types and noises (artificial knock noise and electrical noise). The following conclusions can be drawn.

(1) Different rocks had different rupture features and AE characteristics. The wavelet transform provided a powerful method to acquire the basic characteristics of the rock AE and the environmental noises, such as the energy spectrum and the peak frequency. The signal parameters were input into the network, and the predicted results showed that the wavelet transform method was effective and accurate for AE signal decomposition.

(2) The ANN was proved to be a good method to recognize AE signals from different types of rocks and the environmental noises. The AE signal parameters decomposed by the wavelet transform composed the input layer, the *tansig* function was selected as the transfer function of the hidden layer, and the *logsig* function was selected as the output layer. The average recognition accuracy of the four kinds of rock AE signals was above 95% in the BP neural network.

(3) The signals generated by the granite specimens were much similar to the artificial knock signals. The electrical noises were easy to be recognized by the BP neural network, but it had a low accuracy for the artificial knock noise recognition. To avoid adjacent-channel interference, manmade noises should be reduced as much as possible in laboratory AE tests on rocks.

Conflict of Interests

The authors declare that there is no conflict of interests regarding the publication of this paper.

Acknowledgments

This work was supported by the National Program on Key Basic Research Project of China (973 Program) (Grant nos. 2014CB047100 and 2011CB013503), the National Natural Science Foundation of China (Grant nos. 51374088, 51174071, and 51274053), the Natural Science Foundation of Hebei (E2012209047), the Open Research Fund Program of the State Key Laboratory of Coal Mine Disaster Dynamics and Control (Chongqing University) (2011DA105287-FW201403), and the Scientific Research Projects of Colleges and University in Hebei Province (QN2014067).

References

[1] R. O. Duda, P. E. Hart, and D. G. Stork, *Pattern Classification*, Wiley-Interscience, New York, NY, USA, 2nd edition, 2001.

[2] A. H. Assi, *Engineering Education and Research Using MATLAB*, InTech, Rijeka, Croatia, 2011.

[3] Z.-X. Yang, D.-Q. Feng, T.-J. Chen, and H. Wan, "Application of artificial neural networks to nondestructive testing," *Nondestructive Testing*, vol. 24, no. 6, pp. 244–252, 2002.

[4] R. Yi, S. Liu, and R. Geng, "Application of artificial neural network to acoustic emission testing," *Nondestructive Testing*, vol. 24, no. 11, pp. 488–492, 2002.

[5] C. Bhat, M. R. Bhat, and C. R. L. Murthy, "Acoustic emission characterization of failure modes in composites with ANN," *Composite Structures*, vol. 61, no. 3, pp. 213–220, 2003.

[6] Z. Liang, N. Xu, K. Ma, S. Tang, and C. Tang, "Microseismic monitoring and numerical simulation of rock slope failure," *International Journal of Distributed Sensor Networks*, vol. 2013, Article ID 845191, 10 pages, 2013.

[7] Z. Liang, X. Liu, Y. Zhang, and C. Tang, "Analysis of precursors prior to rock burst in granite tunnel using acoustic emission and far infrared monitoring," *Mathematical Problems in Engineering*, vol. 2013, Article ID 214340, 10 pages, 2013.

[8] P. Lin, Q. B. Li, and P. Y. Jia, "A real-time temperature data transmission approach for intelligent cooling control of mass concrete," *Mathematical Problems in Engineering*, vol. 2014, Article ID 514606, 10 pages, 2014.

[9] P. Lin, Q. B. Li, and H. Hu, "A flexible network structure for temperature monitoring of a super high arch dam," *International Journal of Distributed Sensor Networks*, vol. 2012, Article ID 917849, 10 pages, 2012.

[10] T.-H. Yi, H.-N. Li, and X.-D. Zhang, "Sensor placement on Canton Tower for health monitoring using asynchronous-climb monkey algorithm," *Smart Materials and Structures*, vol. 21, no. 12, Article ID 125023, pp. 1–12, 2012.

[11] T.-H. Yi, H.-N. Li, and M. Gu, "Optimal sensor placement for structural health monitoring based on multiple optimization strategies," *The Structural Design of Tall and Special Buildings*, vol. 20, no. 7, pp. 881–900, 2011.

[12] J.-S. Kwak and J.-B. Song, "Trouble diagnosis of the grinding process by using acoustic emission signals," *International Journal of Machine Tools and Manufacture*, vol. 41, no. 6, pp. 899–913, 2001.

[13] C. Leone, G. Caprino, and I. de Iorio, "Interpreting acoustic emission signals by artificial neural networks to predict the residual strength of pre-fatigued GFRP laminates," *Composites Science and Technology*, vol. 66, no. 2, pp. 233–239, 2006.

[14] I. Grabec and E. Kuljanić, "Characterization of manufacturing processes based upon acoustic emission analysis by neural networks," *CIRP Annals: Manufacturing Technology*, vol. 43, no. 1, pp. 77–80, 1994.

[15] J.-S. Kwak and M.-K. Ha, "Neural network approach for diagnosis of grinding operation by acoustic emission and power signals," *Journal of Materials Processing Technology*, vol. 147, no. 1, pp. 65–71, 2004.

[16] B. Samanta and K. R. Al-Balushi, "Artificial neural network based fault diagnostics of rolling element bearings using time-domain features," *Mechanical Systems and Signal Processing*, vol. 17, no. 2, pp. 317–328, 2003.

[17] B. Samanta, K. R. Al-Balushi, and S. A. Al-Araimi, "Artificial neural networks and support vector machines with genetic algorithm for bearing fault detection," *Engineering Applications of Artificial Intelligence*, vol. 16, no. 7-8, pp. 657–665, 2003.

[18] K. B. Kim, D. J. Yoon, J. C. Jeong, and S. S. Lee, "Determining the stress intensity factor of a material with an artificial neural network from acoustic emission measurements," *NDT and E International*, vol. 37, no. 6, pp. 423–429, 2004.

[19] E. V. K. Hill, P. L. Israel, and G. L. Knotts, "Neural network prediction of aluminum-lithium weld strengths from acoustic emission amplitude data," *Materials Evaluation*, vol. 51, no. 9, pp. 1040–1045, 1993.

[20] R. Wu, Z. Liao, L. Zhao, and X. Kong, "Wavelets application in acoustic emission signal detection of wire related events in pipeline," *Canadian Acoustics*, vol. 36, no. 2, pp. 96–103, 2008.